Journal of Engineering for Development

Journal of Engineering for Development, Vol. 13(2), December (2021) pp.57-66

NUMERICAL ANALYSIS OF TEMPERATURE DISTRIBUTION IN CONTINUOUS SLAB CASTING MOULD

[1]Francis-Akilaki, T.I.; [2]Omoregie, M. J. and [3]Erhunmwun, I.D.

[1,2,3]Department of Production Engineering, University of Benin, Benin City

Email: *[1]tina.odibi@uniben.edu [2]monday.omoregie@uniben.edu, [3]iredia.erhunmwun@uniben.edu*

Abstract

In this paper, the Galerkin Finite Element method was formulated to solve the temperature distribution of the copper mould in continuous slab casting. The method formulates a time dependent problem from the transient heat equation. The pre-heat temperature is 320^{o}C and the molten metal is Grade 1 steel (which contains 0.16% carbon (C), 1.3 % manganase (Mn), 0.5% silicon (Si), 0.05% chromium (Cr), 0.03% mobedium (Mo), and 0.01% tilium (Ti)) with pouring temperature of 1546^{o}C. From the analysis using the 1-D time approximation function it was observed that the temperature of the mould increased as the molten metal is poured into the mould cavity of length 0.65m this is due to heat gained from the molten metal. It was also observed that the mould temperature was highest at the mould length of about 0.075m at a temperature of 490^{o}C and gradually decreases with time and remains in equilibrium at 450^{o}C.

Keywords: *Cotinuous casting, Mould, Temperature distribution*

Article Information:
Received 23 November, 2021
Revised 07 December, 2021
Accepted 10 December, 2021
Available online 08 March, 2022

1.0 Introduction

Michael (2019) defined continuous casting as a process whereby molten metal is solidified into a semi-finished billet, bloom, or slab for subsequent rolling in finishing mills. He further noted that continuous casting process is frequently used to cast not only steel, but also aluminium and copper alloys.

Abuluwefa et. al. (2012) performed a study on the factors encountered in the process of continuous casting, mathematical modeled was carried out by Abuluwafa et. al., (2012) in order to identify the most predominant factors that affects the casting process. These factors modeled are mould thickness, mould material thermal conductivity and molten steel superheat. Simplified calculation were performed in which heat transfer equations governing the process solidification were solved using an explicit method of finite difference technique. From the analysis the results showed that the most effective factor on solidified steel thickness in the mould is the magnitude of molten steel superheat prior to entering the mould. Thermal conductivity of mould material showed little effect due to the small thickness of mould wall. Changing mould thickness showed some effect of solidification but was not significant.

Meng and Brian, 2003 modeled a 1-D transient finite-difference calculation of heat conduction within the solidifying steel shell coupled with 2-D steady-state heat conduction within the mould wall. The model features a detailed treatment of the interfacial gap between the shell and mould, including mass and momentum balances on the solid and liquid interfacial slag layers, and the effect of oscillation marks. The model predicts shell thickness, temperature distributions in the mould and shell, thickness of the re-solidified and liquid powder layers, heat flux profiles down the wide and narrow faces, mould water temperature rise, ideal taper of the mould walls, and other related phenomena.

From various research, it is observed that the Finite difference method and volume of fluid method have been used to solve the heat transfer equation due to conduction in the mould region. This research sort to look at the temperature distribution in the mould using the Galerkin Finite Element method which will significantly increase the accuracy of the results obtained in continuous casting.

2.0 Methodology

Equation 1 is the Fourier heat conduction law equation governing the conductive heat transfer in the mould.

$$q = -kA\frac{\partial T}{\partial x} \tag{1}$$

Where: K = thermal conductivity, A = cross sectional area, T = Temperature
The Fourier heat conduction equation can further be written in a transient form known as the transient heat conduction in a slab (Rajeev K., (2007) as shown in Equation 2

$$\frac{\partial}{\partial x}\left(kA\frac{\partial T}{\partial x}\right)+Ag=\rho CA\frac{\partial T}{\partial t} \tag{2}$$

Where: g = heat energy generated per unit volume, ρ = density, C = specific heat capacity of the material, t = time, A = cross sectional area, x = direction of flow of the molten metal in the x direction

The weak form of equation 2 is developed by multiplying with a weight function (w) and integrated over the domain of interest using a quadratic mesh as shown in equation 3.

$$-\int_{\Omega} w\left[\frac{\partial}{\partial x}\left(k\frac{\partial T}{\partial x}\right)\right]dx+\int_{\Omega} wC\rho\frac{\partial T}{\partial t}dx=0 \tag{3}$$

In writing the final form of the weak form statement, we assume that all boundary conditions at the element level are of the natural type, so that they can be included in the weak form statement as shown in equation 4

$$\int_{x_A}^{x_A+h} k\frac{\partial w}{\partial x}\frac{\partial T}{\partial x}dx+\int_{x_A}^{x_A+h} wC\rho\frac{\partial T}{\partial t}dx-wQ_A-wQ_B=0 \tag{4}$$

Equation 4 is the weak form of the governing equation for temperature distribution in continuous casting.

2.1 Interpolation Function for Continuous Casting

The weak form in Equation 4 requires that the approximation chosen for T should be at least linear in x so that there are no terms in Equation 4 that are identically zero. Since the primary variable is simply the function itself, the Lagrange family of interpolation functions is admissible (Reddy, 2006). We proposed that T is the approximation over a typical finite element domain by the expression:

$$T^e=\sum_{j=1}^{n}T_j^e\psi_j^e(t) \text{ and } w=\psi_i^e(t) \qquad i,j=1,2,3 \tag{5}$$

where $w=\psi_i^e(x)$ is the trial function

In Galerkin's weighted residual method, the weighting functions are chosen to be identical to the trial functions (Reddy, 2006). Substitute Equation 5 into Equation 4, Equation 6 is obtained.

$$k\int_{x_A}^{x_A+h}\frac{\partial\psi_i^e(t)}{\partial x}\frac{\partial}{\partial x}\sum_{j=1}^{n}T_j^e\psi_j^e(t)dx+C\rho\int_{x_A}^{x_A+h}\psi_i^e\frac{\partial}{\partial t}\sum_{j=1}^{n}T_j^e\psi_j^e(t)dx-\psi_i^e(x)Q_A-\psi_i^e(x)Q_B=0 \tag{6}$$

Let $Q_i^e=\psi_i^e(t)Q_A+\psi_i^e(t)Q_B$ (7)

Substituting Equation 7 into Equation 6, Equation 8 is obtained

$$\sum_{j=1}^{n} T_j^e k \int_{x_A}^{x_A+h} \frac{\partial \psi_i^e(t)}{\partial x} \frac{\partial \psi_j^e(t)}{\partial x} dx + C\rho \sum_{j=1}^{n} \frac{\partial T}{\partial t} \int_{z_A}^{z_B} \psi_i^e(t) \psi_j^e(t) dx + Q_i^e = 0 \quad (8)$$

In matrix form, Equation 8 was simplified to obtain Equation 9 which is known as the Finite element based model

$$k\left[K_{ij}^e\right]\left\{T_j^e\right\} + C\rho \dot{T}\left\{M_{ij}^e\right\} = \left\{Q_i^e\right\} \quad (9)$$

where $K_{ij}^e = \int_{x_A}^{x_A+h} \frac{\partial \psi_i^e(t)}{\partial x} \frac{\partial \psi_j^e(t)}{\partial x} dx$ (10)

$$M_{ij}^e = \int_{x_A}^{x_A+h} \psi_i^e(t) \psi_j^e(t) dx \quad (11)$$

Hence, the one-dimensional Lagrange quadratic interpolation Functions used are (equation 12):

$$\psi_1 = \left(1 - \frac{x}{h_e}\right)\left(1 - \frac{2x}{h_e}\right)$$

$$\psi_2 = \frac{4x}{h_e}\left(1 - \frac{x}{h_e}\right) \quad (12)$$

$$\psi_3 = -\frac{x}{h_e}\left(1 - \frac{2x}{h_e}\right)$$

2.2 Evaluating the elemental matrix for continuous casting

2.2.1 Thermal Conductivity $\left[K_{ij}\right]$ matrix

To evaluate the K_{ij} matrix, the elements obtained using Equation 12 were substituted accordingly into equation 10, and obtained Equation 13 which are the values for one element.

$$K^e = \frac{1}{3h_e^3}\begin{bmatrix} 7h_e^2 - 24h_e x_A + 48x_e^2 & -8\left(h_e^2 - 3h_e x_A + 12x_A^2\right) & h_e^2 + 48x_A^2 \\ -8\left(h_e^2 - 3h_e x_A + 12{x_A}^2\right) & 16\left(h_e^2 + 12x_A^2\right) & -8\left(h_e^2 + 3h_e x_A + 12x_A^2\right) \\ h_e^2 + 48x_A^2 & -8\left(h_e^2 + 3h_e x_A + 12x_A^2\right) & 7h_e^2 + 24h_e x_A + 48x_A^2 \end{bmatrix} \quad (13)$$

2.2.2 Enthalpy Matrix $\left[M_{ij}\right]$

To evaluate the M_{ij} matrix, we substituted the elements in equation 12 accordingly into equation 11, and obtained Equation 14 which are the values for one element.

$$M^e = \begin{bmatrix} \frac{\frac{2h_e^4}{15} - h_e^3 x + 3h_e^2 x^2 - 4h_e x^3 + 4x^4}{h_e^3} & \frac{h_e^4 - 30h_e^2 x^2 + 60h_e x^3 - 120x^4}{15h_e^3} & \frac{30h_e^2 x^2 - h_e^4 + 120x^4}{30h_e^3} \\ \frac{h_e^4 - 30h_e^2 x^2 + 60h_e x^3 - 120x^4}{15h_e^3} & \frac{8h_e}{15} + \frac{16x^4}{h_e^3} & -\frac{30h_e^2 x^2 - h_e^4 + 60h_e x^3 + 120x^4}{15h_e^3} \\ \frac{30h_e^2 x^2 - h_e^4 + 120x^4}{30h_e^3} & -\frac{30h_e^2 x^2 - h_e^4 + 60h_e x^3 + 120x^4}{15h_e^3} & \frac{\frac{2h_e^4}{15} + h_e^3 x + 3h_e^2 x^2 + 4h_e x^3 + 4x^4}{h_e^3} \end{bmatrix} \quad (14)$$

2.3 Time approximation for 1-Dimensional Fourier Heat Conduction Equation

Equation 9 can be written in time base form as shown in Equation 15 and the next time step in Equation 16

$$k\left[K_{ij}^e\right]\{T\}_s + C\rho\left[M_{ij}^e\right]\left\{\dot{T}_j\right\}_s = \{Q_i^e\}_s \quad (15)$$

For the next time step $s+1$,

$$k\left[K^e\right]\{T\}_{s+1} + C\rho\left[M_{ij}^e\right]\left\{\dot{T}_j\right\}_s = \{Q^e\}_{s+1} \quad (16)$$

Equation 15 and Equation 16 is multiplied by (1-α) and α respectively, solving further Equation 17 is obtained

$$C\rho\left[M_{ij}^e\right]\left[(1-\alpha)\left\{\dot{T}_j\right\}_s + \alpha\left\{\dot{T}_j\right\}_{s+1}\right] + k\left[K_{ij}^e\right]\left[(1-\alpha)\{T_j\}_s + \alpha\{T_j\}_{s+1}\right] = (1-\alpha)\{Q_i^e\}_s + \alpha\{Q_i^e\}_{s+1} \quad (17)$$

But the α family of interpolation for time consideration is given by Equation 18

$$(1-\alpha)\left\{\dot{T}_j\right\}_s + \alpha\left\{\dot{T}_j\right\}_{s+1} = \frac{\{T_j\}_{s+1} - \{T_j\}_s}{\Delta t_{s+1}} \quad (18)$$

Substituting equation 18 into equation 17 will yield Equation 19

$$\left[C\rho\left[M_{ij}^e\right] + \alpha k\Delta t_{s+1}\left[K_{ij}^e\right]\right]\{T_j\}_{s+1} = \left[C\rho\left[M_{ij}^e\right] - (1-\alpha)k\Delta t_{s+1}\left[K_{ij}^e\right]\right]\{T_j\}_s + \alpha k\Delta t_{s+1}\left[\{Q_i^e\}_s + \{Q_i^e\}_{s+1}\right] \quad (19)$$

Taking the initial condition and $\alpha = 0.5$ as the Crank Nicholson scheme factor Hence equation 19 becomes

$$\left[C\rho\left[M_{ij}^e\right] + k\frac{\Delta t_1}{2}\left[K_{ij}^e\right]\right]\{T_j\}_1 = \left[C\rho\left[M_{ij}^e\right] - k\frac{\Delta t_1}{2}\left[K_{ij}^e\right]\right]\{T_j\}_0 + \frac{\Delta t_{s+1}}{2}\{Q_i^e\}_{s+1} \quad (20)$$

3.0 Result and Discussion

Table 1 shows the design parameters used in analysing the mould.

Table 1: Design and operating parameters used in analysis of the Mould (Alizadeh et. al., 2006)

Preheat Temperature (°C)	320
Mould plate thickness (m x m)	0.043x0.030
Mould length (m)	0.704
Working Mould length (m)	0.659

Mould Copper plate width (m x m)	2.220x0.215
Mould Conductivity k_{mould} (W/mK)	315
Scale thickness on the surface of mould cold surface (m)	0.00001
Mould Powder Conductivity k_{slag} (W/mK)	1.27
Mould powder density $\rho_{slag}\left(kg/m^3\right)$	0.650
Mould Powder Consumption rate M_{slag} (kg/ton steel)	0.8
Copper Mould melting point (^oC)	1084

3.1 Analysis of the mould temperature

In the copper mould heat is transported to the cooling water. Below the mould, cooling is performed by water sprays, by contact with water cooled support rolls, and in the lower part of the machine, by radiation. The mould must be able to extract sufficient heat from the incoming molten steel to solidify a shell which can support the liquid pool at the mould's exit, and thereby minimize breakouts. It is also important for the mould to be able to remove the heat uniformly to avoid the formation of thin regions in the shell which could rupture and lead to breakouts or surface cracks. Therefore, the mould provides support for the newly solidified steel shell at a time when the shell is weak and sensitive to bulging due to ferrostatic pressure.

In the mould region, the analysis is carried out using the initial temperature of the liquid cast 1546^0C at time $t=0$. This temperature represents the Pouring Temperature of the liquid cast. In order to prevent the mould from collapsing due to a sudden change in temperature, the mould was preheated to a temperature of 320^0C which is known as the initial Mould Temperature. The Ambient Temperature before pouring the liquid cast into the mould, the temperature of the air in the mould and outside the mould was taken to be 25^0C.

As the liquid metal is poured into the mould, it is assumed that none of the liquid metal cast solidifies. As the liquid metal is been poured into the mould at the liquid metal/mould interface, the temperature of the liquid metal drops significantly and that of the mould increases significantly.

Figure 2 shows the graph of temperature against the mould length within the liquid metal cast region inside the mould. From the graph, it is observed that as the molten metal is poured into the mould cavity, the temperature of the mould increases due to heat gained from the molten metal poured into the mould cavity, of length 0.65m. It is also observed that the mould temperature is highest at the mould length of about 0.075m and gradually decreases with time and remains in equilibrium. At about 0.075m into the mould, the mould temperature is at its peak of 490^{o}C.

Furthermore from Figure 2 it was observed that the increase in temperature was as result of the molten metal poured into the mould balances up with the temperature as a result of heat withdrawn from the mould due to conduction. Any other point after this peak point, the temperature in the mould begins to drop due to the conductive effect of the mould.

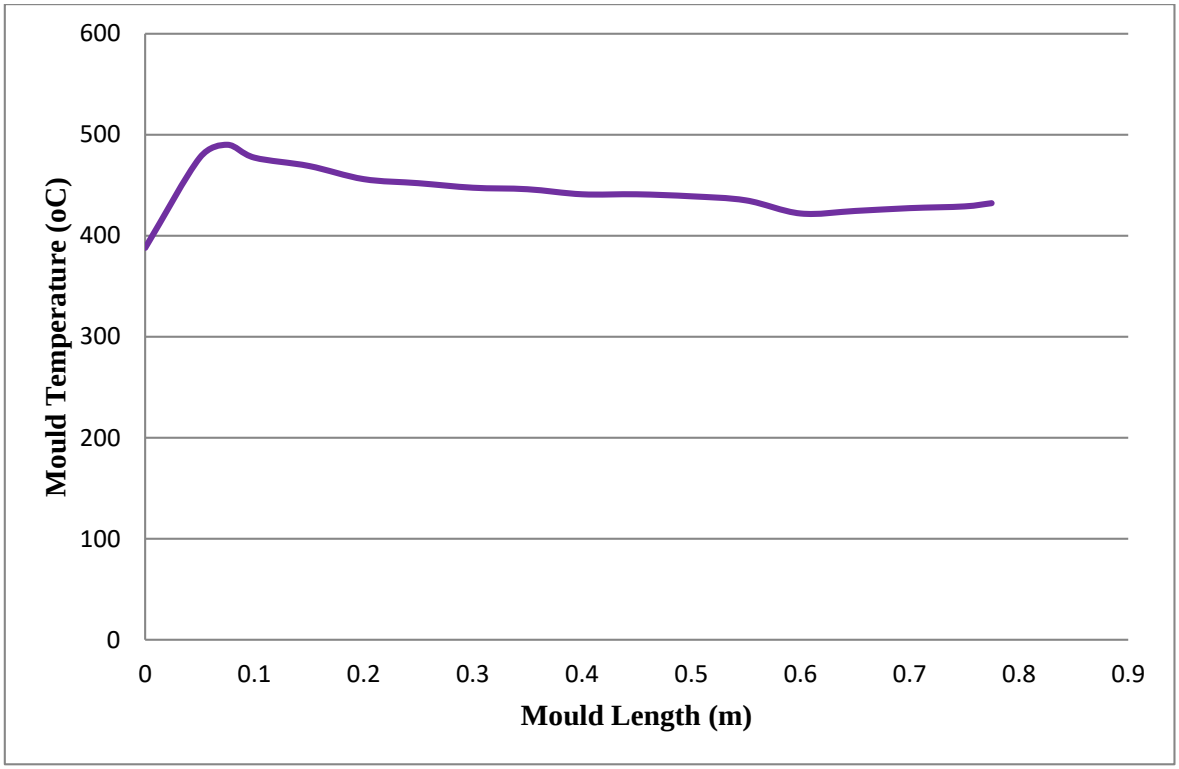

Figure 2: A graph of Mould temperature against mould length

The time approximation equation was solved to evaluate temperature distribution within the mould region for the different process parameters presented. It can be mentioned here that the results obtained using the Finite Element Method in this work are compared with the results obtained in the work of Pooria (2013) using similar conditions.

Figure 3 is the surface plot showing the temperature distribution in the mould region, the yellow patches shows the region of high temperature which surrounds the boundaries of the mould of preheat of 320^{o}C and down to the blue patches of lower than 320.0005^{o}C. At a mould depth of 0.625m the preheat temperature is constant, hence other predictions can be made around the mould when the molten metal is poured in.

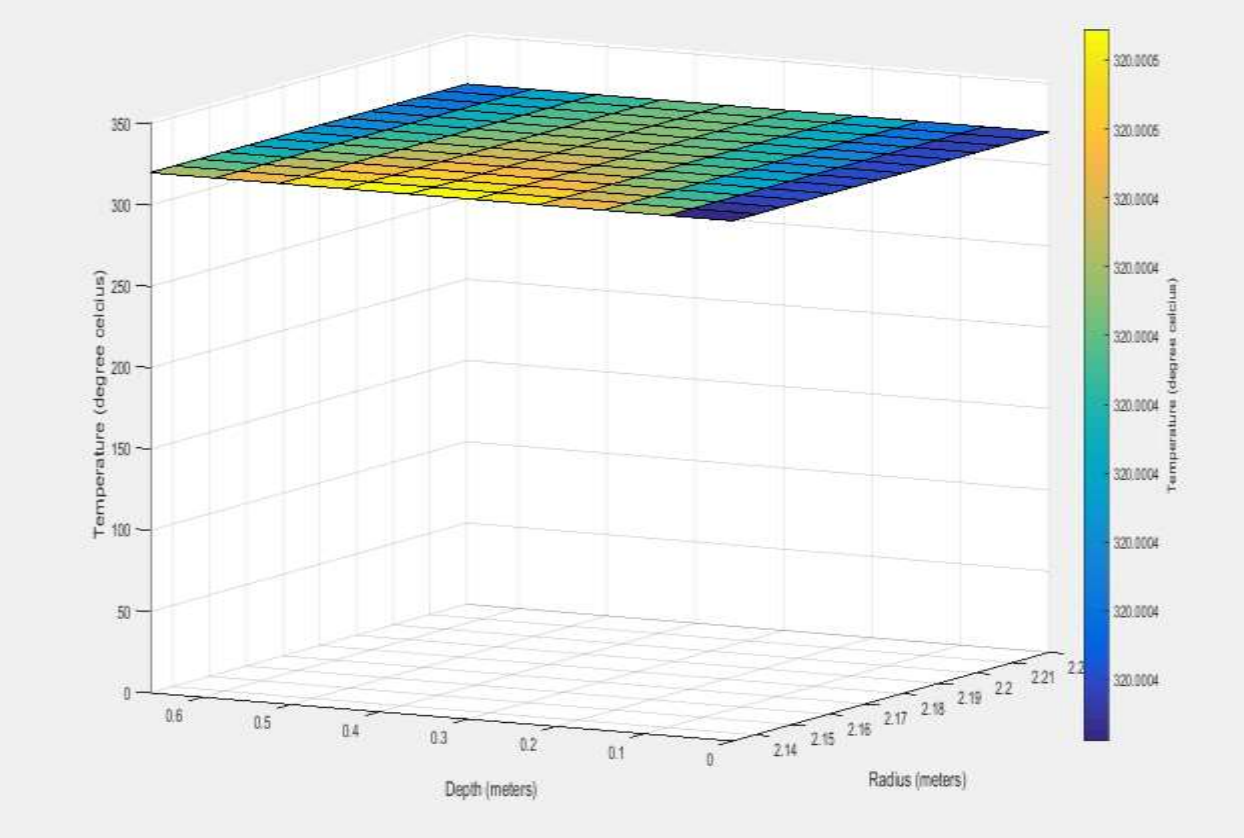

Figure 3: Surface Plot of Mould preheat temperature against mould depth

The contour plot (Figure 4), shows the distribution of the preheat temperature in the mould, it predicts the temperature around the mould depth. The yellow patch shows the region of high temperature which surrounds the boundaries of the mould of 320.005^{o}C and down to the blue patches of lower temperature. At a mould depth of 0.625m the preheat temperature is also constant, hence other predictions can be made around the mould when the molten metal is poured in.

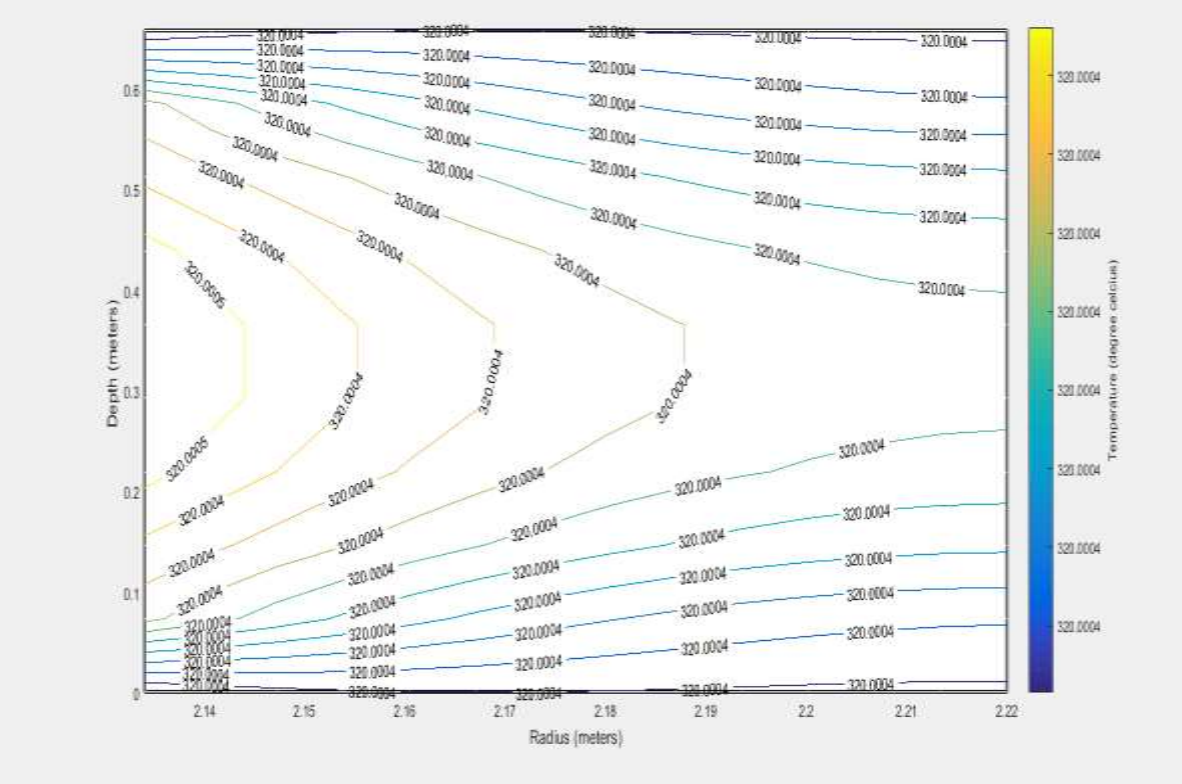

Figure 4: Contour Plot of Preheat temperature distribution in the mould

4.0 Comparison of Results for the Mould

The temperature profile obtained from this research as shown in Figure 2 for the mould shows the peak for the mould temperature of about 490^{o}C and afterward the profile decline gradually along the mould length due to the solidifying shell. This result obtained from the analysis is in agreement with the work of Pooria (2013) as shown in Figure 5.

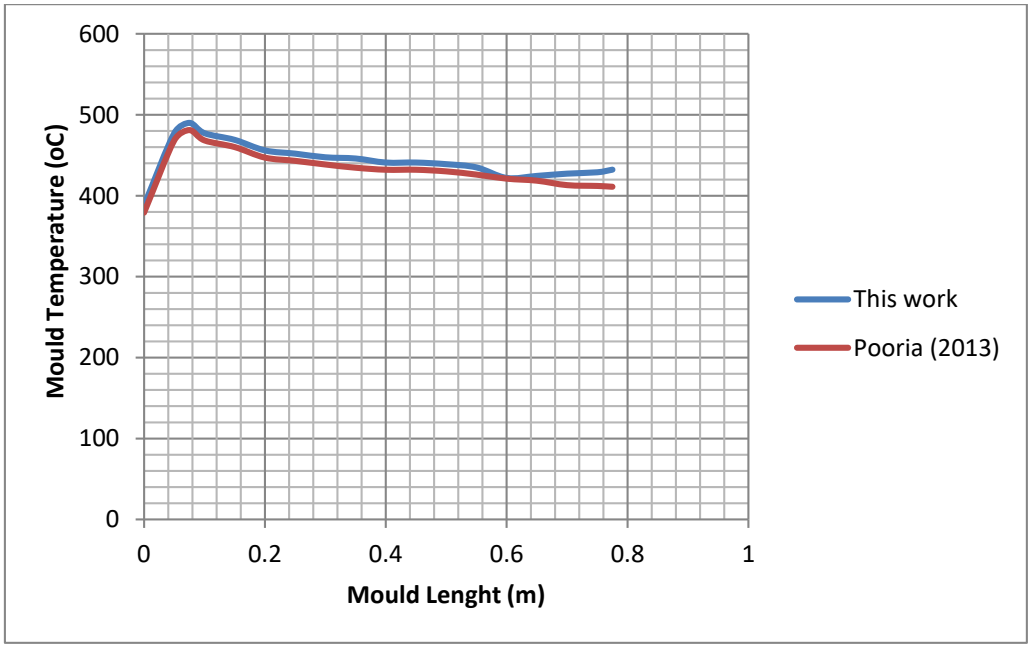

Figure 5: A graph showing the temperature distribution from this work and Pooria (2013) in the mould region

A percentage error analysis was carried out for results obtained from this research and the result obtained by Pooria (2013). The maximum absolute percentage error obtained was 0.0487% at a mould length of 0.775m and the minimum absolute percentage error obtained was 0.0020% at a mould length of 0.6m. This comparison was made for the temperature distribution in the mould region as the molten metal is poured into the mould cavity, the temperature of the mould increases due to heat gained from the molten metal poured into the mould cavity.

5.0 Conclusion

This research was able to determine the temperature distribution numerically of the mould using the Galerkin Finite Element Method. The method used in this research gives a node by node analysis within a given domain which presents a better analysis. The results obtained were validated with results carried out by Pooria (2013). It was observed that the temperature of the liquid metal drops significantly and that of the mould increases significantly due to heat gained from the molten metal poured into the mould cavity of length 0.65m. It was also observed that the mould temperature is highest at the mould length of about 0.075m at a temperature of 490^{o}C.

Reference

Abuluwefa H. T., Al-Ahresh M. A., Bosen A. A. (2012), "Factors Affecting Solidification of Steel in the Mould during Continuous Casting of Steel Billets", Proceedings of the International Multi-Conference of Engineers and Computer Scientists, IMECS, vol. 2, pp: 1-5.

Alizadeh M., Edris H. and Shafyei A. (2006), "Mathematical modeling of heat transfer for steel continuous casting process", International Journal of ISSI, vol. 3(2), pp: 7-16.

Meng Y. and Brian G. T. (2003): "Heat Transfer and Solidification Model of Continuous Slab Casting: CON1D". Metallurgical and Materials Transactions B, Vol. 34B, No. 5, pp. 685-705.

Michael V. (2019), "Continuous casting", MDPI metals, vol. 9 (643), pp: 1-3.

Pooria N. J. (2013), "Analysis of Different Continuous Casting Practices Through Numerical Modelling" Master Thesis, Division of Applied Process Metallurgy, Department of Materials Science and Engineering, KTH Royal Institute of Technology, SE-100 44 Stockholm, Sweden.

Rajeev K., (2007): "Numerical solution of moving boundary problem related to continuous casting". A thesis submitted in partial fulfillment of the requirements for the degree of Master of Technology in the Department of Mechanical Engineering National Institute of Technology Rourkela.

Reddy J. N. (2006): An introduction to the finite element method, Mcgraw-Hill, Third Edition, Texas.